R. F. S. Andrade, G. Dewel, and P. Borckmans
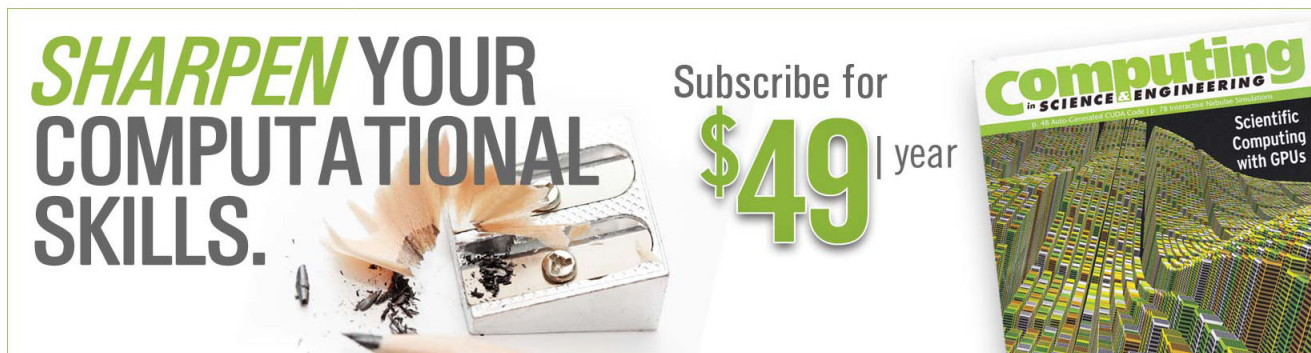
Modeling of the kinetic oscillations in the CO oxidation on Pt(100)

R. F. S. Andrade,[a] G. Dewel,[b] and P. Borckmans[b]

Service de Chimie-Physique, C.P. 231, Université Libre de Bruxelles, 1050 Bruxelles, Belgium

We analyze a model recently introduced by Imbihl *et al.* to describe the kinetic oscillations in the catalytic oxidation of CO on Pt(100). However we describe the surface reconstruction by a time dependent Ginzburg–Landau equation. With realistic values of the rate constants the region of oscillations in the $P_{CO} \times P_{O_2}$ diagram extends to very low values of the partial pressures ($P_{CO} = 1.5 \times 10^{-6}$ Torr, $P_{O_2} = 2.7 \times 10^{-5}$ Torr) in agreement with the experimental results. In the investigation of the critical points and of the dynamics it has been possible to identify both saddle-node infinite period (SNIPER) and Hopf bifurcations.

I. INTRODUCTION

Kinetic oscillations in heterogeneously catalyzed reactions have now been observed in a large variety of systems and conditions.[1] The origin of these temporal behaviors is still investigated intensively. In the case of the catalytic oxidation of CO on well-defined Pt(100) or Pt(110) single crystal surfaces, these oscillations could be traced back to the coupling between the catalytic activity and a structural modification of the surface.[2-5] The rate constants (adsorption, desorption, reaction) which determine the surface coverage strongly depend upon the arrangement of the surface metal atoms. On the other hand, in these systems a critical coverage can induce a reconstruction of the surface. This mechanism provides the necessary feedback loop which will produce the instability. It is indeed well known that such open systems when driven sufficiently far from equilibrium may exhibit oscillatory behavior and even develop spatial (dissipative) structures.[6] More recently it has been suggested that the oscillations observed on polycrystalline wires and foils and on supported Pt particles may also arise from an adsorbate induced phase transition.[7]

Pt(100) presents two main states: (1) the quasihexagonal ("hex") structure which is stable at low coverages has no catalytic activity since the corresponding oxygen sticking coefficient is very low (10^{-3} to 10^{-4}); (2) the catalytic active 1×1 structure analog to that of the bulk is stabilized in the presence of an adsorbed layer. LEED observations have shown that the surface transforms periodically between these two states during the oscillations in the production of CO_2.[2]
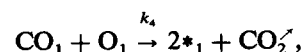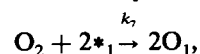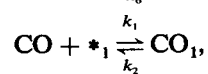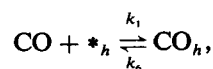
These phenomena have been theoretically investigated with the help of a mathematical model of four differential equations whose numerical solutions qualitatively reproduce some of the experimental observations.[3] In this work we extend this description by introducing two modifications in the quoted model. The first one refers to the description of the adsorption of O_2 on the 1×1 phase. It is well known that O_2 adsorption is inhibited by the CO preadsorbed layer. On the other hand it is favored by the presence of surface defects which may be of two different kinds: crystalline defects and irregularities in the CO adlayer. When the latter are properly taken into account a better agreement between experiment and theory can be achieved. The second modification conerns the description of the adsorbate induced phase transition. The corresponding driving force is the energy gained by the CO adsorption on the 1×1 patches. Using a simple lattice model[8] we have obtained approximate expressions for the free energy of the surface states. As a result we have derived a Ginzburg–Landau equation to describe the dynamics of this surface transformation. This modification is convenient for the analysis of the dynamical behavior of the model.

The rest of the paper is organized as follows. In Sec. II we discuss the kinetic model stressing upon the modifications we have introduced. In Sec. III we study the fixed points of the model and discuss their stability. Section IV presents a discussion of the trajectories in phase space which have been obtained by the numerical integration of the equations of motion. Section V closes the paper with a discussion of our results and further comments.

II. THE KINETIC MODEL

It has been shown that the catalytic oxidation of CO on Pt proceeds by a bimolecular Langmuir–Hinshelwood reaction between the adsorbed species.[9] An essential feature of the model is the strong dependence of O_2 adsorption on both the surface structure and the CO surface coverage. The sticking coefficient of O_2 on the hex phase is indeed very small and the inhibiting effect of CO preadsorption is well documented. The kinetics of the surface transformation and the migration of the adsorbed CO molecules from the hex to the 1×1 patches (the so-called trapping) must thus be added to the Langmuir–Hinshelwood mechanism. We are thus lead to the following steps[3]:

$$CO + *_h \underset{k_6}{\overset{k_1}{\rightleftharpoons}} CO_h,$$

$$CO + *_1 \underset{k_2}{\overset{k_1}{\rightleftharpoons}} CO_1,$$

$$O_2 + 2*_1 \overset{k_7}{\rightarrow} 2O_1,$$

$$CO_1 + O_1 \overset{k_4}{\rightarrow} 2*_1 + CO_2',$$

---

[a] Permanent address: Instituto de Física, Universidade Federal da Bahia, Brazil.
[b] Research Associates to the Belgium Fund for Scientific Research.

$$CO_h + *_1 \xrightarrow{k_3} CO_1 + *_h,$$

$$*_h \rightleftharpoons *_1, \tag{2.1}$$
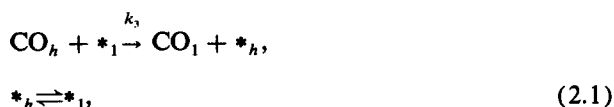
where $*$ symbolizes a free adsorption site and the indices h and 1 refer, respectively, to the hex and 1×1 phases.

In the absence of mass transfer limitations, mass balance of the various surface species produce the following evolution equations[3]:

$$du_a/dt = ak_1 P_{CO} - k_2 u_a + k_3 a u_b - k_4 u_a v_a/a, \tag{2.2}$$

$$du_b/dt = (1 - a)k_1 P_{CO} - k_3 a u_b - k_6 u_b, \tag{2.3}$$

$$dv_a/dt$$
$$= k_7 P_{O_2} a [(1 - sv_a/a - ru_a/a)^2 + \alpha(1 - sv_a/a)^2]$$
$$- k_4 u_a v_a/a, \tag{2.4}$$

where u_a, u_b, and v_a are the fractions of surface sites occupied by CO on 1×1 and hex phases and O_2 on 1×1; a is the fraction of the surface sites in the 1×1 phase and the k_i are the rate constants defined in Eq. (2.1). In the model, one assumes that the flow rates are sufficiently high so that the partial pressures can be assumed constant.

On the other hand, s, r, and α are parameters related to the adsorption of O_2. As already pointed out there is a strong inhibition in the adsorption of O_2 due to the presence of preadsorbed O and CO. Reasonable experimental values are $s = 5/3$ and $r = 2$. Conversely there is an enhancement of the adsorption due to the presence of surface defects which are of two types. The first one refers to crystalline defects in the surface of the metal as kinks, vacancies,.... STM observations have indeed shown that the surface transformation is accompanied by considerable microscopic roughening of the surface.[10] This kind of defect which is independent of the extension of the preadsorbed layer is described by the parameter α. Defects of a second type are those caused by irregularities in the preadsorbed layer. Their presence is uncovered by LEED investigations of the adlayer through the presence of a $c(4,2)$ pattern in addition to the regular $c(2,2)$.[11] That pattern appears when the CO coverage is very close to its inhibiting value 0.5 for O_2 adsorption and it shows that the density of these defects depends on the coverage. We assume hereafter that $r = 2/(1 + \beta)$ where $\beta > 0$ accounts for this second type of defects.

The system (2.2)–(2.4) has now to be completed by a fourth equation describing the dynamics of a. A surface reconstruction is a very complex phenomenon in particular when there is no group–subgroup relation between the symmetry groups of the two phases. For this purpose we consider a simple lattice model describing the interactions of the Pt surface atoms with the bulk Pt atoms ($H_i^{(1)}$) and with the adsorbed layer ($H_i^{(2)}$) as well as the interactions between nearest-neighbor sites of the surface ($H_{ij}^{(3)}$). The corresponding Hamiltonian then takes the form

$$H = \sum_i H_i^{(1)}(\phi_i) + \sum_i H_i^{(2)}(\phi_i) + \sum_{ij} H_{ij}^{(3)}(\phi_i,\phi_j). \tag{2.5}$$

We describe the transition by means of a discrete variable ϕ_i which can assume the values 0, 1/2, or 1 according to

whether the surface atom is in a patch of hex phase, on the border between hex and 1×1 patches or in the 1×1 phase and another variable n_i which is the occupation number of the ith adsorption site. The explicit forms of the terms in Eq. (2.5) are

$$H_i^{(1)}(\phi_i) = \begin{cases} 0 & \text{if } \phi_i = 0 \\ \gamma & \text{if } \phi_i = 1/2, \\ \delta & \text{if } \phi_i = 1 \end{cases} \tag{2.6}$$

$\gamma > \delta > 0$ in order to take into account the observed differences of activation energy between the hex and (1×1) phases. Their values are obtained from Fig. 9 of Ref. 12. We define the zero of energy as the energy of the clean Pt hex surface:

$$H_i^{(2)}(\phi_i) = - \epsilon_h n_i (1 - \phi_i) - \epsilon_1 n_i \phi_i, \tag{2.7}$$

where ϵ_h and ϵ_1 describe the lowering of energy due to the adsorption of gas molecules on the patches of hex and 1×1 phase[12] (their values are taken from Table I of Ref. 3) and

$$H_{ij}^{(3)}(\phi_i,\phi_j) = \epsilon [\phi_i(\tau - \phi_j) + \phi_j(\tau - \phi_i)]. \tag{2.8}$$

The parameter ϵ is a measure of the strength of the interaction. Concerning τ, we note that when it equals one, the lowest interaction energy (i.e., zero) occurs when both nearest-neighbors sites are either in the hex or in the 1×1 phases. For $\tau \neq 1$ this symmetry between the two phases is broken and the lowest energy occurs when the two sites are in the hex phase. We have neglected the interaction between adsorbate molecules as we think that these contributions are not directly related to the phase transition. We also define the mean coverages

$$U_a + V_a = \sum_i \langle n_i \phi_i \rangle / N_1$$

and

$$U_b = \sum_i \langle n_i(1 - \phi_i) \rangle / N_h.$$

If we further introduce $a = \Sigma_i \langle \phi_i \rangle / N$, a mean field expression for the free energy of the above model can be evaluated using standard techniques.[21] We find

$$g(T,a) = - kT [\text{Log}[D(1 - a) + AR] - 2a \text{ Log } R$$
$$- 2(1 - a)\text{Log}(1 - a)]$$
$$+ \delta(2a - 1) + z\epsilon a(\tau - a)$$
$$- U_b \epsilon_h (1 - a) - (U_a + V_a)\epsilon_1 a, \tag{2.9}$$

where z is the number of nearest neighbors and

$$A = \exp(-\gamma/kT)/2, \quad D = \exp(-\delta/kT),$$
$$R = A(a - 0.5) + [A^2(a - 0.5)^2 + Da(1 - a)]^{1/2}. \tag{2.10}$$

The equation of motion for a is therefore

$$da/dt = - k_8 \frac{1}{\epsilon_1} dg/da$$
$$= k_8 \left[U_a + V_a - \frac{\epsilon_h}{\epsilon_1} U_b - kT F(T,a) \right], \tag{2.11}$$

where $F(T,a)$ is easily computed from Eq. (2.9). The fol-

lowing relations also hold: $U_a = u_a/a, V_a = v_a/a$, and $U_b = u_b/(1-a)$ as in Ref. 3. The model is now complete. However it entails a great number of parameters and rate constants whose values strongly influence the dynamical behavior. The experimental values of the rate constants k_1, k_2, k_4, k_6, k_7, and k_8 are rather precisely determined.[3] A good fit for k_3 has been derived from a study of the CO/Pt system. The parameters α and β are limited to small values, usually $\alpha, \beta < 0.4$. The lattice model (2.6)–(2.8) contains seven parameters. $\gamma, \delta, \epsilon_h$, and ϵ_1 can be determined from the experimental study of the energetics of the hex to 1×1 transformation.[11,12] So we are left with the values of ϵ and τ which can be choosen so that the model conveniently describes the experimental features of the CO/Pt system ($P_{O_2} = 0$).

Pronounced hysteresis effects are observed when the temperature is increased and decreased at constant CO pressure.[12,13] We have thus determined the optimal values of ϵ and τ for which the model reproduces the hysteresis loops as shown in Fig. 1(a). The value of all the parameters are gathered in Table I.

In the next section we undertake an analysis of the fixed points of the model. For this purpose, the cumbersome expression for $g(T,a)$ [Eq. (2.9)] may in general be expanded in terms of the order parameter a:
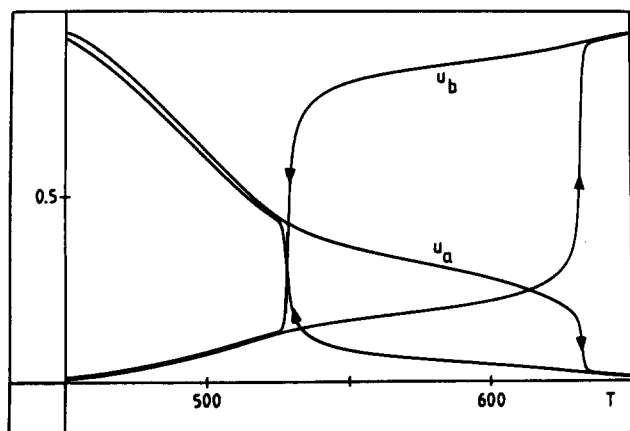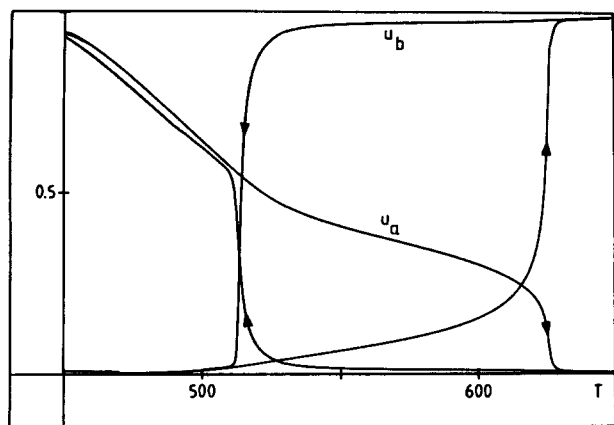
TABLE I. Parameter values.

Constant	Experimental value ($T = 480$ K)	Value in this work
k_1	2.35×10^5 ML s^{-1} Torr^{-1}	2.35×10^5 ML s^{-1} Torr^{-1}
k_2	9×10^{-3}–1.5 s^{-1}	1 s^{-1}
k_3	50 ± 30 s^{-1}	50 s^{-1}
k_4	10^3–10^5 ML^{-1} s^{-1}	10^3–10^5 ML^{-1} s^{-1}
k_6	11 s^{-1}	10 s^{-1}
k_7	5.6×10^4 ML s^{-1} Torr^{-1}	5.6×10^4 ML s^{-1} Torr^{-1}
k_8	0.4–2 s^{-1}	1 s^{-1}
α	$\cdots$	0.25
β	$\cdots$	0.25
γ	2.3×10^{-19} J	2.3×10^{-19} J
δ	6.9×10^{-20} J	2.5×10^{-20} J
ϵ_h	1.9×10^{-19} J	3.4×10^{-20} J
ϵ_1	2.3×10^{-19} J	4.1×10^{-20} J
z	4–6	4–6
ϵ	$\cdots$	3.25×10^{-20} J
τ	$\cdots$	0.65

$$g_{GL}(T,a) = \epsilon_1(U_a + V_a)a + \eta_2(T)a^2 + \eta_3(T)a^3 + \eta_4(T)a^4. \tag{2.12}$$

It is indeed well known that it is possible to represent a first order transition by truncating the series (2.12) after the fourth order term (Ginzburg–Landau potential).[14] For the parameters values shown in Table I and temperatures in the range of interest, it turns out that the following values of the η_i fit the results quite well:

$$\eta_2 = 2, \quad \eta_3 = -10/3, \quad \eta_4 = 7/4.$$

A comparison between $g(T,a)$ and $g_{GL}(T,a)$ (for $U_a = U_b = V_a = 0$) is shown in Fig. 2. Moreover it follows from the model and the values of the rate constants that U_b is always small. So if we approximate $g(T,a)$ by the Ginzburg–Landau potential and take $U_b = 0$, the equation of motion for a becomes

$$da/dt = k_8[U_a + V_a - 4a + 10a^2 - 7a^3]. \tag{2.13}$$

This simplified model (2.2)–(2.4) and (2.13) also reproduces the hysteresis loops as shown in Fig. 1(b).

FIG. 1. (a) Temperature hysteresis loop for the CO coverage on 1×1 (u_a) and the fraction of sites in the hex phase (u_b) obtained by integration of Eqs. (2.2), (2.3), and (2.11). (b) The same situation but with Eq. (2.13) replacing Eq. (2.11).
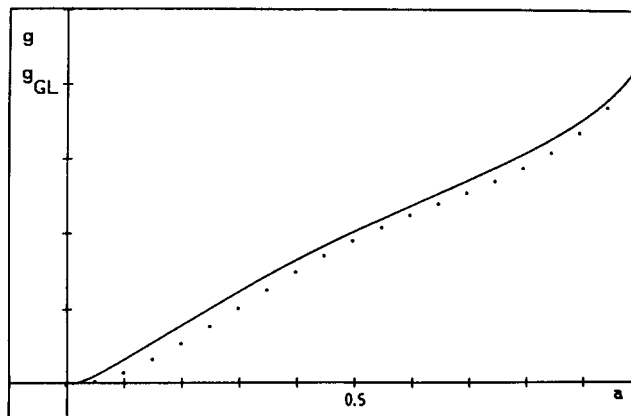
FIG. 2. Surface free-energy for the lattice models (2.5)–(2.9). The full line is the temperature average (450–650 K) of Eq. (2.9) and the dots indicate the Ginzburg–Landau potential (2.12).

In summary we stress that we have introduced two new features in the model: the influence of the inhomogeneities in the adsorption layer and a kinetic equation describing the dynamics of the surface transformation. Clearly, our lattice model does not include all the possible interactions. However it is interesting to see that this simple description already reproduces rather well the experimental hysteresis loops of the CO/Pt system. This is a support for using it to investigate the more complex situation when $P_{O_2} \neq 0$.

III. FIXED POINTS ANALYSIS

Using the local concentrations U_a, U_b, and V_a, the stationary states of the system are the solutions of

$$k_1 P_{CO} - k_2 U_a + k_3 (1 - a) U_b - k_4 U_a V_a = 0, \quad (3.1)$$

$$k_1 P_{CO} - k_6 U_b - k_3 a U_b = 0, \quad (3.2)$$

$$k_7 P_{O_2} [(1 - sV_a - rU_a)^2 + \alpha(1 - sV_a)^2] - k_4 U_a V_a = 0, \quad (3.3)$$

$$U_a + V_a - 4a + 10a^2 - 7a^3 = 0. \quad (3.4)$$

Substituting U_b and V_a, respectively obtained from Eqs. (3.1) and (3.2), into the two remaining equations, U_a and a are the solutions of the system formed by Eq. (3.4) and

$$4p_O U_a^4 + 4\beta'(k_2 - p_O + sp_O k_2/k_4)U_a^3$$
$$+ \beta'^2(\alpha'p_O - \bar{p}_C + 2\alpha'sp_O k_2/k_4$$
$$+ sp_O \bar{p}_C/k_4 + \bar{p}_C s^2 k_2^2/k_4^2)U_a^2$$
$$- \beta'^3(\alpha'\bar{p}_C sp_O/2k_4 + \alpha'\bar{p}_C s^2 p_O k_2/2k_4^2)U_a$$
$$+ \beta'^4 \alpha'\bar{p}_C s^2 p_O/16k_4^2 = 0, \quad (3.5)$$

where

$$p_O = 2rk_7 P_{O_2}; \quad \bar{p}_C = p_C(1 + q)/(1 + aq);$$
$$p_C = 2rk_1 P_{CO}; \quad q = k_3/k_6; \quad (3.6)$$
$$\alpha' = 1 + \alpha; \quad \beta' = 1 + \beta.$$

To proceed further one must resort to numerical analysis. It may however be substantiated here owing to the fact that k_4 is much larger than the other parameters (see Table I). Indeed the polynomial (3.5) may be factored in the limit $k_4 \to \infty$ into two second degree equations the solutions of which are

$$U_0^\pm = \frac{1}{k_4} \frac{s\bar{p}_C}{2r} \frac{1}{1 \mp (\bar{p}_C/\alpha'p_O)^{1/2}} + O(k_4^{-2}), \quad (3.7)$$

$$U_1^\pm = \{1 - k_2/p_O \pm [(1 - k_2/p_O)^2 + \bar{p}_C/p_O - \alpha']^{1/2}\}/r + O(k_4^{-1}). \quad (3.8)$$

If we keep p_O constant and increase p_C we note that when

$$\bar{p}_C \simeq \alpha'p_O \quad (3.9)$$

the solution U_0^+ increases without bound, whereas U_1^+ goes to zero if $1 - k_2/p_O < 0$ (if $1 - k_2/p_O > 0$ then U_1^- goes to zero and the situation is the same). The condition (3.9) implies that the coefficient of U_a^2 in Eq. (3.5) is of the order of k_4^{-1}. In this situation, the solutions U_0^+ and U_1^+ (or U_1^-) are not the roots of Eq. (3.5) any more. They are replaced by

$$U_2^\pm = \frac{k_4^{-1/2}}{r} \frac{-\Delta \pm [\Delta^2 + 8\alpha' s\bar{p}_C p_O(k_2 - p_O)]^{1/2}}{4(k_2 - p_O)}, \quad (3.10)$$

where

$$k_4^{1/2}(\alpha'p_O - \bar{p}_C) = \Delta \simeq 1.$$

The solutions (3.10) correspond to a situation where both U_a and V_a are of the order of $k_4^{-1/2}$. When p_C is increased beyond the value corresponding to Eq. (3.9), expression (3.7) is valid again, but U_0^+ is now negative and can be disregarded.

From the above discussion we see that, for practical purposes, the steady states corresponding to low CO coverages are limited to values of p_c lower than that given by Eq. (3.9). Moreover, in that neighborhood U_a, $V_a \propto k_4^{-1/2}$ and as a consequence the solution of Eq. (3.4) is $a \propto k_4^{-1/2}$. It follows from the definition (3.6) that the solutions U_0^+ are limited to the region

$$p_O \geqslant \frac{p_C}{\alpha'} \frac{1+q}{1+aq} = \frac{p_C}{\alpha'}(1+q) + O(k_4^{-1/2}). \quad (3.11)$$

To study the linear stability properties of the fixed points we have to find the eigenvalues of the Jacobian matrix of the system (2.2)–(2.4) and (2.13).

For the fixed point U_0^+ it turns out that the approximate existence condition (3.11) is very close to the actual stability region and in fact we will not distinguish between them hereafter. For the fixed points $U_1^\pm$ the situation is more complex. Equation (3.4) with $U_1^\pm$ in place of U_a and $V_a \propto k_4^{-1}$ may have up to seven roots. When $p_O \leqslant 2$ we can always find at least one solution which is stable. When p_O increases above this value there are some ranges of values of p_C where no stable solution exists. So in order to draw the borderline of the region where at least one fixed point $U_1^\pm$ is stable we have to investigate the stability of all branches of solutions. The presence of at least one stable fixed point for given values of p_C and p_O indicates that the system may be found in a stationary state. On the other hand, if no stable fixed point exists (for given p_C and p_O) we infer that the system will be in a oscillatory or chaotic state. The way the fixed points become unstable determines the type of bifurcation at the threshold to the oscillatory region. For the present model there are both Hopf and SNIPER (saddle-node infinite period) bifurcations,[15] which will be discussed in the next section.

To close this section we present a $p_O \times p_C$ phase diagram in Fig. 3 where the stability regions of the fixed points U_0^+ and U_1^+ are drawn. The parameter values are those of Table I. This figure may be compared with the experimental $P_{CO} \times P_{O_2}$ diagrams.[16] They are in agreement with respect to the presence of three regions characterized by: (i) CO over hex and O over 1×1 steady state; (ii) CO over 1×1 steady state; and (iii) oscillatory behavior. The lower bounds for the oscillatory region are $p_C = 1.5$ and $p_O = 2.5$, or $P_{CO} = 2 \times 10^{-6}$ Torr and $P_{O_2} = 1.33 \times 10^{-5}$ Torr which are in quantitative agreement with experimental results.

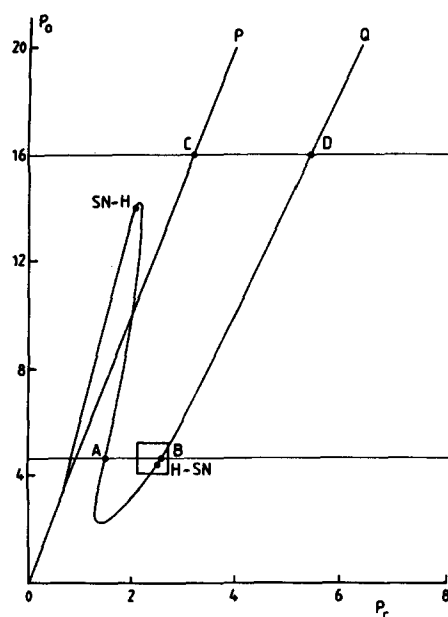We note also that there is a coexisting region where both

FIG. 3. The $p_C \times p_O$ phase diagram: The region above OP admits stable fixed points (FP) with small u_a and a. That below OQ has FP with large u_a and a. The region in between has no stable FP and oscillatory behavior occurs. At the line OP saddle-node bifurcations take place. At OQ we have saddle-node (SN) bifurcation from 0 to point SN–H and from H–SN to Q. Between SN–H and H–SN we have again Hopf bifurcation. Points A, B, C, and D indicate conditions which are discussed in Sec. IV. Oscillations may also occur where stable FP and limit cycle coexist, e.g., close to point H–SN.

fixed points corresponding to low (U_0^+) and high (U_1^+) CO coverages on the 1×1 phase exist and are stable. In this region the value of a is of the same order ($\simeq 0.1$) for both fixed points: the surface is in the hex phase, but the remaining 1×1 sites may be covered either by O or CO. This latter possibility, the "finger" at low p_C which extends into high p_O values, has not been found in the parameter region covered by the experiments.

We also recall that the oscillatory region in our diagram is characterized by the absence of stable fixed points. Hence we do not exclude that time dependent behavior may occur outside that region.

IV. TRAJECTORIES IN PHASE SPACE/DYNAMICAL BEHAVIOR

In this section we analyze the dynamics of the system (2.2)–(2.4) and (2.13) for some values of the partial pressures P_{CO} and P_{O_2} near the bifurcations where oscillations set in.

The investigation of the stability of the fixed points of Sec. III showed that the linear stability matrix has, around each fixed point, one eigenvalue $\lambda_1 \simeq - k_4$ and another negative eigenvalue $\lambda_2 \simeq - (k_6 + ak_3)$ the value of which depends on a. The other two eigenvalues have rather complex dependences on the parameters of the system and may become critical for some values of the partial pressures.

It follows that the dynamics of the system along the direction of the first eigenvector is a rapid relaxation. Also

when $a \gg k_4^{-1/2}$, $\lambda_2 \simeq - 50$ and the decay is also comparatively fast along the direction of the corresponding eigenvector. It is thus feasible to carry through an adiabatic elimination of these fast relaxing variables and bring the original model into a two-dimensional system of differential equations which makes it easier to characterize the various dynamical behaviors. If on the other hand $a \lesssim k_4^{-1/2}$ at the bifurcation point then $\lambda_2 \simeq - 10$ and the reduction is still possible although the quality of the approximation becomes poorer.

Thus if we let

$$w = u_a - v_a + aqu_b/(1 + aq),$$
$$y = u_a - v_a - aqu_b/(1 + aq),$$ (4.1)
$$z = u_a + v_a$$

and eliminate y and z adiabatically as

$$y = w + O(1/k_6 + ak_3),$$
$$z = \pm (w + y)/2 + O(1/k_4),$$ (4.2)

we get the following:

$$dw/dt = ak_1 P_{CO} (1 + q)/(1 + aq)$$
$$- k_2(w + |w|) - ak_7 P_{O_2}$$
$$\times \{[1 - (r - s)w/2a - (r + s)|w|/2a]^2$$
$$+ \alpha[1 - s(w - |w|)/2a]^2\}$$
$$+ O(1/k_6 + ak_3),$$ (4.3)

$$da/dt = k_8[|w|/a - 4a + 10a^2 - 7a^3] + O(1/k_6 + ak_3).$$ (4.4)

The two possibilities for z in Eq. (4.2) are due to the form of the dominant term in the equation used for the elimination of z [$z^2 = (w + y)^2/4$]. They are related to the situation with high ($+$) and low ($-$) CO coverages on the 1×1 phase. The corrections indicated in Eqs. (4.2) and (4.3) may be carried through in a straightforward way, although the expressions we arrive at have a very cumbersome form.

The system (4.3) constitutes a good approximation for our original model. This is shown by the properties of its fixed points which are much the same as those discussed in the last section and also by the comparison of the trajectories in phase space which are obtained by numerical integration as we will present hereafter.

The numerical integration of the trajectories was performed by means of a fourth order Runge–Kutta routine on a HP-9386 microcomputer. For the system (2.2)–(2.14) the typical step of integration Δt must be less than $1/k_4$. Thus we took the value $k_4 = 1000$ (what causes the relaxation time to increase but does not change the kind of dynamics) and $\Delta t = 10^{-4}$. For the system (4.2) Δt may be much larger.

In Fig. 4 we plot the time development of the four variables for different values of P_{CO} and P_O, corresponding to different bifurcating situations. These correspond to the points A, B, C, and D as indicated in Fig. 3. Point A is near a line of Hopf bifurcations. Thus the oscillations are characterized by small amplitude and sinusoidal shape with slowly varying period as P_{CO} changes, as illustrated in Fig. 4(a). By increasing P_{CO} this typical shape changes very quickly into
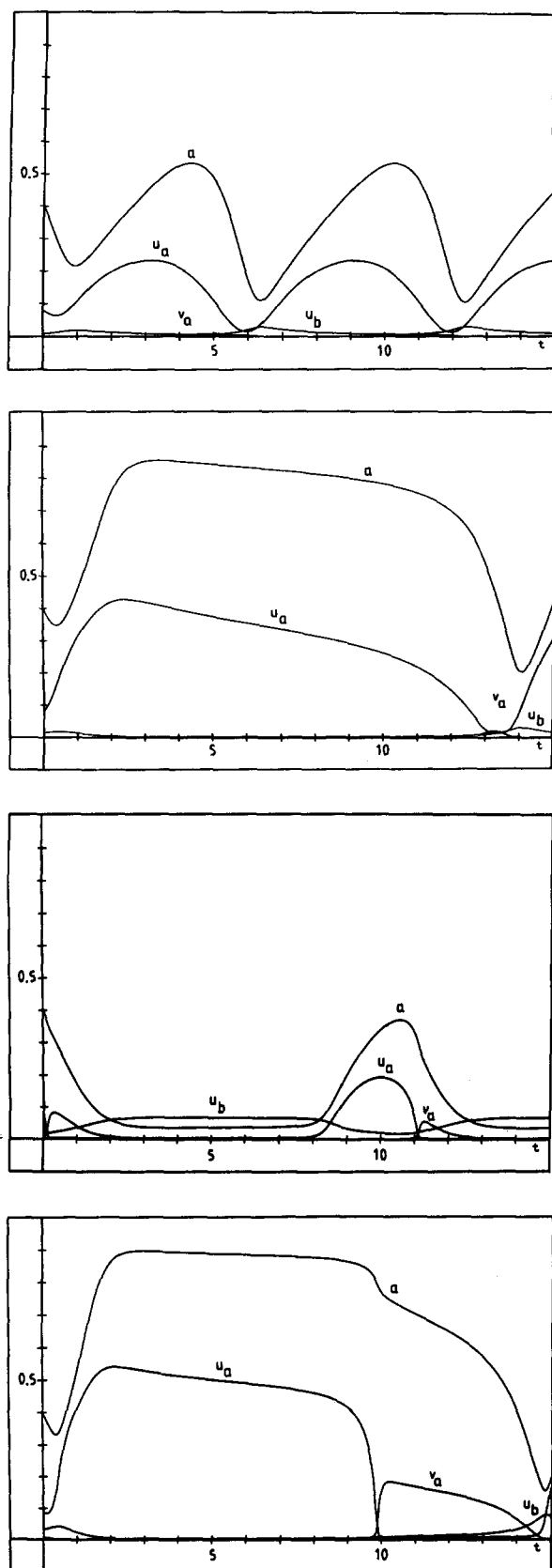
relaxation oscillations, which are very characteristic of the recorded experimental data. After a further increase in P_{CO} we approach point B. It belongs to a line which is indicated in Fig. 3 to be characterized by SNIPER bifurcations. Indeed the period of oscillations starts to increase without bounds when we come closer to B, as it may be inferred from Fig. 4(b). This is the distinguishing feature of a SNIPER bifurcation in contrast to other saddle-node bifurcations. This behavior is related to the occurrence of a homoclinic trajectory[17] to a fixed point. This is a global change in the structure of the phase space that cannot be detected by a local analysis of the fixed points as presented in the last section. No general analytical method is available for the identification of homoclinic orbits, which are generally found by numerical computations. Later in this section we will present a closer discussion of the situation close to point B based on the integration of the system (4.2).

For a higher fixed value of P_O, we arrive at the oscillatory region upon increasing P_{CO} by crossing the line given by Eq. (3.9) where saddle-node bifurcations occur. The numerical integration of the trajectories for parameter values close to point C in Fig. 3 also shows that we have a SNIPER bifurcation, as inferred by Fig. 4(c). Finally Fig. 4(d) shows another situation (point D in Fig. 3) at the same line of SNIPER bifurcations as point B. We observe only slight changes in the shape of the oscillations with respect to Fig. 4(b). For instance we note that the O_2 coverage (V_a) reaches a higher value which reshapes the plateau of the variable a.

Let us now make a finer discussion of the SNIPER bifurcation taking place along the line OQ close to point B of Fig. 3. To that purpose we make use of the system (4.3). First of all we show in Fig. 5 a time development of w and a for the same parameter values as in Fig. 4(b). The comparison of the trajectory for a in both figures shows that a rather good agreement is achieved after the adiabatic elimination. It becomes still better if a higher value of k_4 is used in the integration of the system (4.2)–(4.14).

Close to point B the bifurcations which take place along the line OQ change from Hopf into SNIPER type. This is due to the fact that for that range of parameter values there
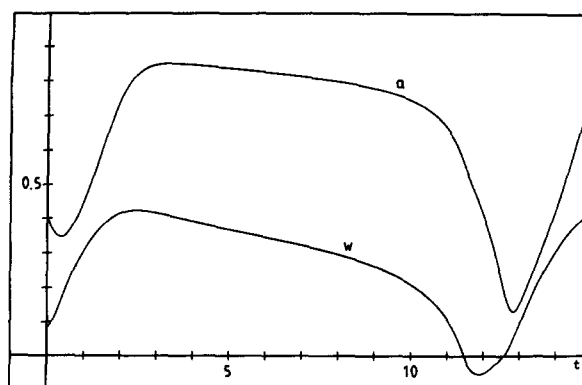
FIG. 4. Time evolution of the four variables u_a, u_b, v_a, and a for various (p_C, p_O) values. These are shown so that the system is in the oscillatory region of Fig. 3 and close to the points A(a), B(b), C(c), and D(d). Conditions: $k_2 = 1$, $k_3 = 50$, $k_4 = 1000$, $k_6 = 10$ and (a) $p_C = 1.6$, $p_O = 4.6$, (b) $p_C = 2.49$, $p_O = 4.6$, (c) $p_C = 2.66$, $p_O = 16$, (d) $p_C = 5.33$, $p_O = 16$. Times are expressed in seconds and $\alpha = 0.25$.

FIG. 5. Time evolution for the variables w and a of the reduced system (4.2) for the same conditions (p_C, p_O) as in Fig. 4(b). Times are expressed in seconds.

are up to three fixed points which are located very closely to each other in the phase space. The situation is illustrated in Fig. 6 which is a blow-up of the region near point B in the phase diagram. Thus for values of P_O smaller than P_{O1} we leave the oscillating region on increasing the value of P_{CO} by means of a Hopf bifurcation. This one is followed by the emergence of a saddle-node pair. Later on the saddle will collapse with the node emerging from the stable focus which originated from the Hopf bifurcation. Decreasing P_O eventually leads to a critical point $C1$ which causes the cusp that terminates the SN curve.

For values of P_O larger than P_{O1} the saddle-node pair will appear before the Hopf bifurcation. Therefore, for a small interval of values of P_{CO} there will be two attractors: the stable node and the limit cycle which will vanish at the Hopf bifurcation. This phase portrait is illustrated in Fig. 7(a). In our Fig. 3 we assigned this coexistence region as nonoscillatory for one cannot warrant that oscillations will really set in. As a second comment we mention that this situation is not yet typical of a SNIPER bifurcation. This situation will occur only for higher values of P_O. Now the line of Hopf bifurcations is not so close to the SN line, and the radius of the limit cycle at the SN line is larger. When the radius is large enough, the limit cycle extends itself until the place where the saddle-node pair emerges. In this circumstance it becomes a homoclinic loop to the fixed point and the period of oscillations goes to infinity. Figures 7(b) and 7(c) illustrate the occurrence of two (stable) homoclinic trajectories. Eventually the Hopf line meets the SN curve at the $C2$ codimension two bifurcation point. We have not studied the dynamical behavior near this point. To conclude we recall that these three different schemes go into one another in a very narrow interval of values of P_O, what may cause its experimental identification to be very difficult.
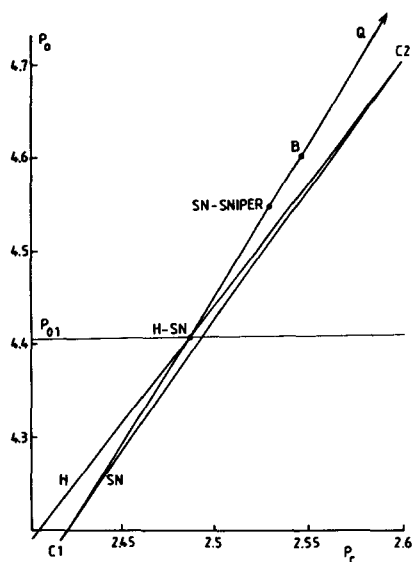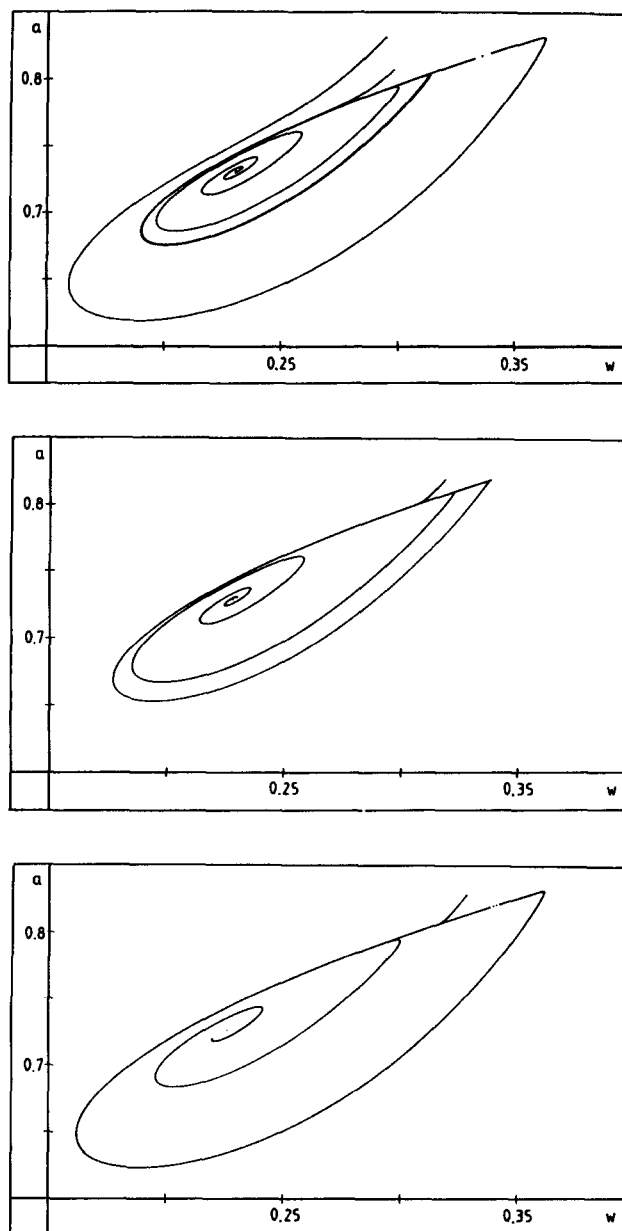

FIG. 7. Phase space trajectories of the system (4.2) for parameters values in the same range as in Fig. 6. In (a) the stable limit cycle and the collapsing saddle-node pair (dot with $a > 0.8$) coexist. The situation corresponds to the SN line below the SN–SNIPER point in Fig. 6. On the other hand (b) and (c) show homoclinic trajectories on the SN line at the point SN–SNIPER and above [in (c) the dots with $a > 0.8$ represent the collapsing saddle-node pair].

FIG. 6. Enlargement of the $p_c \times p_O$ phase diagram corresponding to the window around point H–SN in Fig. 3. H and SN indicate the lines of Hopf and saddle-node bifurcations. At the point H–SN itself the border of the oscillatory region changes over from Hopf to saddle-node bifurcations. Above the point SN–SNIPER there exists a homoclinic orbit to the collapsing saddle-node pair and infinite period bifurcation sets in.

V. CONCLUSION

The main results of this paper are well summarized in Fig. 3 which exhibits the boundaries of the oscillatory domain in the $P_{CO} \times P_{O_2}$ diagram in good agreement with the experimental observations. It is again important to stress that the stability properties of the fixed points strongly depend on the value of the parameter β we have introduced to describe the influence of the inhomogeneities in the CO adlayer. The diagram presented in Fig. 3 could not be reproduced by taking $\beta = 0$ and varying the value of α.

We have described the kinetics of the surface phase transformation by means of a Ginzburg–Landau equation. The form of the corresponding free energy has been motivated by a simple lattice model describing the microscopic interactions on the surface and the various parameters have been fitted to reproduce the hysteretic behavior exhibited by the CO/Pt system. The use of a Ginzburg–Landau functional in this nonequilibrium problem is based on the reasonable assumption that the observed surface structures (hex and 1×1) correspond to local minima of a coarse-grained free energy which includes the surface concentrations (U and V) determined by the various rate processes (surface reactions, adsorption–desorption, and trapping). The other degrees of freedom relax rapidly for each phase structure (local equilibrium). The variation of these nonequilibrium surface concentrations then provides the driving mechanism for the transition.

The use of this kinetic equation has allowed the characterization of the nature of the bifurcations leading to oscillatory behavior. In particular, by numerical integration of the trajectories, infinite period bifurcations have clearly been identified for some values of the parameters; the transition from oscillatory to steady state behavior is accompanied by a dramatic increase of the period. Andronov et al.[15] have pointed out that there are four types of instabilities leading to stable periodic orbits; super- and subcritical Hopf bifurcations, SNIPER, and saddle-loop bifurcations. The possibility of occurrence of SNIPER bifurcation in chemical systems has recently given rise to much investigations, see Ref. 18 and references therein; it is thus interesting to have a further realistic chemical model which may exhibit this kind of instability. Relaxation experiments could be performed in that region to try and observe the signature of these instabilities.

Next it would be highly desirable to study the nature of the spatial patterns which have been observed by LEED on single crystals during the oscillations in the gas phase.[2]

Two types of periodic chemical waves have indeed been identified in oscillating systems: (1) target patterns[19] generated by a local modification of the oscillating frequency induced by an impurity (here an excess of defects) or a fluctuation; (2) traveling waves appearing through a primary symmetry breaking instability.[20] Two modifications must then be introduced in the model used above. One must take into account the surface diffusion of the adsorbed CO molecules. The oxygen atoms are so tightly bound to the surface that their surface diffusion can be ignored.[9] A gradient term[14] must also be introduced in the Ginzburg–Landau functional. It is associated to the increase in free energy due to the formation of an island of one phase into the other one (interfacial energy). Work in this direction is in progress.

[1] L. F. Razon and R. A. Schmitz, Catal. Rev. Sci. Eng. **28**, 89 (1986).
[2] M. P. Cox, G. Ertl, and R. Imbihl, Phys. Rev. Lett. **54**, 1725 (1985).
[3] R. Imbihl, M. P. Cox, G. Ertl, H. Müller, and W. Brenig, J. Chem. Phys. **83**, 1578 (1985).
[4] R. Imbihl, M. P. Cox, and G. Ertl, J. Chem. Phys. **84**, 3519 (1986).
[5] H. Eiswirth and G. Ertl, Surf. Sci. **177**, 90 (1986).
[6] G. Nicolis and I. Prigogine, *Self-Organization in Nonequilibrium Systems* (Wiley, New York, 1977).
[7] S. B. Schwartz and L. D. Schmidt, Surf. Sci. **183**, L269 (1987).
[8] V. P. Zhdanov and K. I. Zamaraev, Sov. Phys. Usp. **29**, 755 (1986).
[9] G. Ertl, in *Catalysis, Science and Technology*, edited by J. R. Anderson and M. Boudart (Springer, Berlin, 1983), Vol. 4, p. 209.
[10] R. J. Behm, W. Hösler, R. Ritter, and G. Binnig, Phys. Rev. Lett. **56**, 228 (1986).
[11] R. J. Behm, P. A. Thiel, P. R. Norton, and G. Ertl, J. Chem. Phys. **78**, 7437 (1983).
[12] P. A. Thiel, R. J. Behm, P. R. Norton, and G. Ertl, J. Chem. Phys. **78**, 7448 (1983).
[13] T. E. Jackman, K. Griffiths, J. A. Davis, and P. R. Norton, J. Chem. Phys. **79**, 3529 (1983).
[14] L. Landau and E. Lifshitz, in *Statistical Physics*, 3rd. ed., edited by E. Lifshitz and L. Pitaevskii (Pergamon, Oxford, 1984), Part 1.
[15] A. A. Andronov, A. A. Vitt, and J. E. Khaikin, *Theory of Oscillators* (Pergamon, Oxford, 1966).
[16] H. Eiswirth, R. Schwankner, and G. Ertl, Z. Phys. Chem. N. F. **144**, 59 (1985).
[17] J. Guckenheimer and P. Holmes, *Nonlinear Oscillations, Dynamical Systems, and Bifurcations of Vector Fields*, Appl. Math. Sci. **42** (Springer, Berlin, 1983).
[18] V. Gaspar and K. Showalter, J. Chem. Phys. **88**, 778 (1988).
[19] Y. Kuramoto, *Chemical Oscillations, Waves, and Turbulence*, Synerget. Ser. **24** (Springer, Berlin, 1984).
[20] L. M. Pismen, Phys. Rev. A **23**, 334 (1981).
[21] R. P. Feynman, *Statistical Mechanics* (W. A. Benjamin, Reading, Mass., 1972).